Biomedical Physics & Engineering
Express

ENDORSED BY
IPEM Institute of Physics and Engineering in Medicine

ACCEPTED MANUSCRIPT

Gradient image smoothing for metal artifact reduction (GISMAR) in computed tomography

To cite this article before publication: Yakdiel Rodriguez-Gallo *et al* 2019 *Biomed. Phys. Eng. Express* in press https://doi.org/10.1088/2057-1976/ab0c4d

Manuscript version: Accepted Manuscript

Accepted Manuscript is “the version of the article accepted for publication including all changes made as a result of the peer review process, and which may also include the addition to the article by IOP Publishing of a header, an article ID, a cover sheet and/or an ‘Accepted Manuscript’ watermark, but excluding any other editing, typesetting or other changes made by IOP Publishing and/or its licensors”

This Accepted Manuscript is **© 2018 IOP Publishing Ltd**.

During the embargo period (the 12 month period from the publication of the Version of Record of this article), the Accepted Manuscript is fully protected by copyright and cannot be reused or reposted elsewhere.
As the Version of Record of this article is going to be / has been published on a subscription basis, this Accepted Manuscript is available for reuse under a CC BY-NC-ND 3.0 licence after the 12 month embargo period.

After the embargo period, everyone is permitted to use copy and redistribute this article for non-commercial purposes only, provided that they adhere to all the terms of the licence https://creativecommons.org/licences/by-nc-nd/3.0

Although reasonable endeavours have been taken to obtain all necessary permissions from third parties to include their copyrighted content within this article, their full citation and copyright line may not be present in this Accepted Manuscript version. Before using any content from this article, please refer to the Version of Record on IOPscience once published for full citation and copyright details, as permissions will likely be required. All third party content is fully copyright protected, unless specifically stated otherwise in the figure caption in the Version of Record.

View the article online for updates and enhancements.

This content was downloaded from IP address 129.110.242.50 on 13/03/2019 at 10:15

Gradient image smoothing for metal artifact reduction (GISMAR) in computed tomography

Yakdiel Rodríguez-Gallo[1], Rubén Orozco-Morales[2], Marlen Pérez-Díaz[2]

Abstract

Metal artifacts can impair accurate diagnosis, and degrade the image quality and diagnostic value of CT-slices. In this work we propose a novel gradient image smoothing for metal artifact reduction (GISMAR) algorithm for image quality improvement in patients with hip implants, dental fillings, DBS implants and permanent seed implants. Using Image Smoothing via L0 Gradient Minimization method, a global thresholding method, and the principle of NMAR method, the authors developed a new MAR method that does not depend on access to raw projection data. To validate the authors' approach, 2D-CT data from twenty-two patients with different metal implants were used and processed by GISMAR and three more well- known algorithms. In order to evaluate metal artifact reduction, mean CT number (HU and SD) was calculated as well as a subjective analysis with three expert observers. Image quality on images was compared using the non-parametric Friedman-ANOVA test. We conclude that GISMAR method can efficiently reduce metal artifacts using CT-slice, does not introduce new artifacts, while preserving anatomical structures.

Keywords: Computed tomography; metal artifact reduction; implants; image quality

[1] Departamento de Electrónica y Telecomunicaciones, Univ. Central 'Marta Abreu' de Las Villas, Cuba.

[2] Departamento de Automática y Sistemas Computacionales, Univ. Central 'Marta Abreu' de Las Villas, Cuba.

Abbreviations and acronyms

CPU	Central Processing Unit
CT	Computed Tomography
FBP	Filtered Back Projection
FP	Forward Projection
FSNMAR	Frequency Split Normalized Metal Artifact Reduction
GE	General Electric
GISMAR	Gradient Image Smoothing for Metal Artifact Reduction
GLP	Gaussian Low-Pass

Accepted Manuscript

HU	Hounsfield Units
L0GM	L0 Gradient Minimization
LI	Linear Interpolation
MAR	Metal Artifact Reduction
NMAR	Normalized Metal Artifact Reduction
SD	Standard Deviation

INTRODUCTION

Artifacts due to metallic implants are common in Computed Tomography (CT) images as a result of beam-hardening, scatter effects and photon-starvation [1–3]. Over the last four decades, a lot of algorithms have been developed to reduce metal artifacts. These metal artifact reduction (MAR) algorithms can be divided mainly into five classes: Acquisition Improvement, Physics-based Pre-processing, Projection Completion, Iterative Reconstruction and Image-based Approaches [4]. In order to improve the acquisition process, dual-energy protocols have been proposed [5, 6]. A number of MAR techniques have been developed based on the assumption that the projections associated with the metal objects are completely missing or corrupted and are useless for CT-slice reconstruction. The incomplete data are completed by interpolations among the assumed useful measured data. Linear [7–9] or polynomial [10, 11] interpolation techniques can be used for this purpose.

Other algorithms use a normalization step [12–14] to improve projection completion processes. Additionally, some iterative reconstruction methods have been developed to reduce metal artifacts [15–19]. On the other hand, a small proportion of methods prefer to handle the artifacts in the image domain [20]. In these methods, artifacts are reduced after the image has been reconstructed.

The purpose of this study is present the preliminary results obtained by a new MAR method (GISMAR). The novelty of this new MAR is that eliminate the need to access to the raw projection data from the CT scanner; working directly on two-dimensional CT-slices. Consequently, this method could be implemented in a dedicated software for using in workstations and personal laptops. GISMAR method uses Image Smoothing via L0 Gradient Minimization (L0GM) method [21], Isoentropic based on Global Thresholding method [22, 23] and the principle of normalized metal artifact reduction (NMAR) method [12] to interpolate in the sinogram domain. Image quality was compared with four well-known algorithms: filtered back projection (FBP), linear interpolation (LI), NMAR and frequency split normalized metal artifact reduction (FSNMAR). The advantages of our method are demonstrated using clinical dataset.

Accepted Manuscript

MATERIALS AND METHODS

Metal artifact reduction approaches

In this study, three well-known MAR methods were selected to compare the performance of GISMAR method. The first algorithm selected was LI [24]. Although, this method reduces the artifacts, new ones are induced. NMAR algorithm proposed by Meyer et al. [12] was the second algorithm chosen. To maintain the size and the edges of the metal implant, both methods, LI and NMAR, reinsert the metal image from the originally reconstructed image in the final corrected image. In addition, to improve the edge information of surrounding bone structures the application of FSNMAR algorithm was introduced by Meyer et al [13], being the third algorithm selected in this research. The thresholds for the segmentation of metal were set according to the paper [13] for LI, NMAR and FSNMAR in this work. For full details of these algorithms, please refer to corresponding literature.

Algorithm developed

The GISMAR algorithm uses various steps of data segmentation. A flow diagram for the GISMAR algorithm is shown in Figure 1.

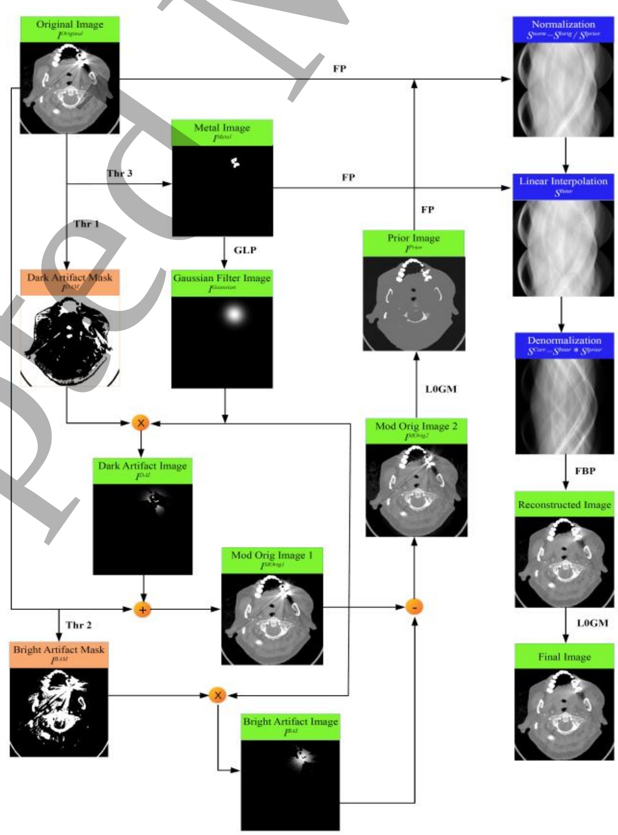

Accepted Manuscript

Fig. 1. Flow diagram showing the steps of the gradient image smoothing for metal artifact reduction (GISMAR) algorithm.

As a first step, the artifacts were automatically segmented from the FBP reconstructed CT-slice ($I^{Original}$) using the previously published Isoentropic based Global Thresholding method by Bianconi *et al.* [22, 25], for automatic thresholding-based segmentation. Methods based on entropy, like the Isoentropic, has the advantage of being able to discriminate between types of objects according to their information content. In MAR, the most widely implemented segmentation method employs global thresholding, whereby a global threshold is used to distinguish the metal from the non-metal objects in the image. However, several studies have claimed that minor segmentation errors may have significant detrimental effects on the overall performance of the MAR method [26]. New studies on this topic will be published in the future by GISMAR authors.

When the Isoentropic method is applied to the $I^{Original}$, threshold (*Thr1*) is obtained. This threshold is used to obtain the dark artifact mask (I^{DAM}), as is shown in Figure 1. This threshold is multiplied by a factor (*ThF1*) and *Thr2* is obtained. This new threshold was used to get the bright artifact mask (I^{BAM}). Both I^{DAM} and I^{BAM} are binary images. These images were yielded to segment the dark and bright artifacts in $I^{Original}$, and recover the lost structures. Subsequently, *Thr3* is gotten multiplying *Thr2* by a factor *ThF2 (Thr1 < Thr2 < Thr3)*. In this case, *Thr3* is used to segment the metallic implants in the original image, obtaining the metal image (I^{Metal}). It should be noted that *Thr1* is calculated automatically through Isoentropic method for each CT-slice, and it will vary mainly depending on the anatomical structure analyzed according to its position in the human body. *ThF1* factor can be varied between 1.6 and 1.8; and *ThF2* between 3.9 and 4.2. It is recommended to use a *ThF1* value of 1.7 and *ThF2* of 4.1 for implants as presented in this paper. These were found experimentally.

Once a metal image is obtained (I^{Metal}), a strong smoothing by a Gaussian low-pass (GLP) filter is used to obtain the Gaussian filtered image ($I^{Gaussian}$). A GLP with size of 200 x 200 pixels and a SD of σ ≈ 25 pixels was used. $I^{Gaussian}$ contains the local average intensity level, so, when it is combined with I^{DAM} and I^{BAM}, the local average intensity level is recovered, obtaining the dark artifact image (I^{DAI}) and bright artifact image (I^{BAI}). The modified original image 1 (I^{MOrig1}) is the result of adding the image I^{DAI} to $I^{Original}$. From the result of this mathematical operation is subtracted the image I^{BAI}, obtaining the modified original image 2 (I^{MOrig2}). I^{MOrig2} contains all the information from $I^{Original}$. I^{MOrig2} was obtained, using the following equation:

$$I^{MOrig2} = I^{Original} + \left(I^{DAM} * I^{Gaussian}\right) - \left(I^{BAM} * I^{Gaussian}\right) \quad (1)$$

In order to obtain a prior image (I^{Prior}) (Fig. 1), a L0GM [21] is applied to the I^{MOrig2}. This method was selected based on the mechanism for discretely counting spatial changes, because it can remove low-

Accepted Manuscript

amplitude structures and globally preserve and enhance outgoing edges, even if they are boundaries of very narrow objects. Additionally, it has been used due to its characteristics and benefits in medical imaging [27, 28].

In L0GM, λ is the smoothing parameter, which controls the degree of smoothing, and κ controls the iterations rate. Five iterations are generally performed in the algorithm to obtain a good I^{Prior}, with $\kappa = 1.8$. We recommend using a λ value of 1×10^{-5} in dataset as used in this work. These iterations are carried out because I^{Prior} cannot have artifacts. The goal is to discriminate artifacts from real structures in the original image so that we can replace artifact contaminated regions of the original image with tissue values by interpolation; and the discrimination is used to reduce metal artifacts [29, 30]. A high λ value is applied in order to achieve a deep smoothing, eliminating the artifacts that exist in I^{MOrig}, and thus obtaining an optimal I^{Prior} without artifacts and with the most tissue information from the $I^{Original}$.

Sinograms from $I^{Original}$, I^{Prior} and I^{Metal} were obtained using forward projection (FP). FP was carried out using parallel-beam geometry. Following the method developed by [12], the original sinogram is normalized (S^{Norm}) by dividing it by the sinogram of the I^{Prior} pixelwise. Moreover, all values from the S^{Norm} that lie within the metal trace (I^{Metal}) are replaced in each row by linear interpolation (See Kalender et al. [24] for further details). Afterwards, the corrected sinogram (S^{Corr}) is obtained by denormalization of the interpolated (S^{Inter}).

Finally, the reconstructed image (I^{Rec}) is obtained using FBP with linear interpolation and a ramp filter from S^{Corr}. This image is then processed using L0GM again with two iterations ($\kappa = 1.8$ and $\lambda = 9 \times 10^{-5}$). In this step, the parameters of the L0GM were selected to achieve a soft smoothing, and bring out the edges and fine anatomical structures, as well as eliminate some remaining streak artifacts due to noise, obtaining the final image (I^{Final}).

Patients

The authors had complete control of the data in the article submitted for publication. The images used from a GE Medical Systems CT were employed in previous research [31]. Additionally, the other dataset was approved by Institutional Review Board in the hospital where it was obtained. Informed consent was obtained from all these patients. The study was performed by using the DICOM images from CT datasets obtained in 22 adults (mean age 61.5 years; range 21–84 years). The main inclusion criterion was the presence of a metallic implant in the examination area. The only exclusion criterion was to have an age under 18 years. The mean patient's weight was 65.8 ± 10 kg (range 39.2–97.5 kg). Only the image data of the patients was used in the study, keeping all other patient's information anonymous.

Image acquisition

Accepted Manuscript

The CT datasets were obtained for this research from two different CT scanners: GE Medical Systems CT and a Siemens SOMATOM Sensation 16 scanner CT using helical scanning geometry. Patients with dental fillings were scanned on a GE CT with a filter type “Body filter”, convolution kernel “standard”, Slice Thickness 2.5 mm, Tube current 250 mA and kilovolt peak 120 kV; in the case of patients with hip implants with “Body filter”, convolution kernel “standard”, Slice Thickness 2.5 mm, tube current 440 mA and kilovolt peak 120 kV; and of patients with seed implants, a filter type “Body filter”, convolution kernel “B30s”, Slice Thickness 2.5 mm, Tube current 139 mA and kilovolt peak 130 kV. Others patients with dental fillings were scanned on a Siemens SOMATOM Sensation 16 scanner CT and it utilized a filter type “WEDGE_2”, convolution kernel “'H31s”, Tube current 226 mA and kilovolt peak 120 kV. On the other hand, patients with DBS implants were scanned on a Siemens SOMATOM Sensation 16 scanner CT, being used a filter type “WEDGE_2”, convolution kernel “'H31s”, Tube current 256 mA and kilovolt peak 140 kV. The matrix size of the reconstructed images was 512 x 512 pixels in both scanners. Corresponding pixel sizes were 1 mm X 1 mm for GE CT and 0.776 mm X 0.776 mm for Siemens SOMATOM Sensation. The CT datasets were taken from different anatomical regions and had the following distribution: three seed implants, three hip implants and three dental implants acquired from GE CT; eleven dental fillings and two DBS implants from Siemens SOMATOM Sensation.

Image analysis

Clinical images obtained by using FBP, LI, NMAR, FSNMAR and GISMAR were independently evaluated by three board-certified Radiologists, each with more than ten years of experience, and blind to all patient data and image parameters. Images were visualised under the same conditions; displayed in random order. Images were displayed using a 23” LED backlight monitor with a 1920 x 1080 resolution. Observers viewed the monitors from an approximate viewing distance of 2-2.5 screen heights. Experiments were conducted in dimmed ambient light (less than 25 lux).

Statistical Analysis

In the objective comparison, in order to assess the quantitative capability of the GISMAR algorithm for metallic artifact reduction, two regions of interest (ROIs) were drawn on the original and the processed CT images. CT numbers (HU) and standard deviations (SD) were measured by two radiologists within the 2 ROIs selected by them, one strongly affected and the second weakly affected by metallic artifacts. The position of ROI is dependent on each image. Three examples of this ROI location are shown in figure 2. The size (4 mm2) and shape (circular) of the ROIs were maintained for all measurements. This size was not so small as to be affected by pixel variability. Figure 2 shows some examples indicated by red circles.

Accepted Manuscript

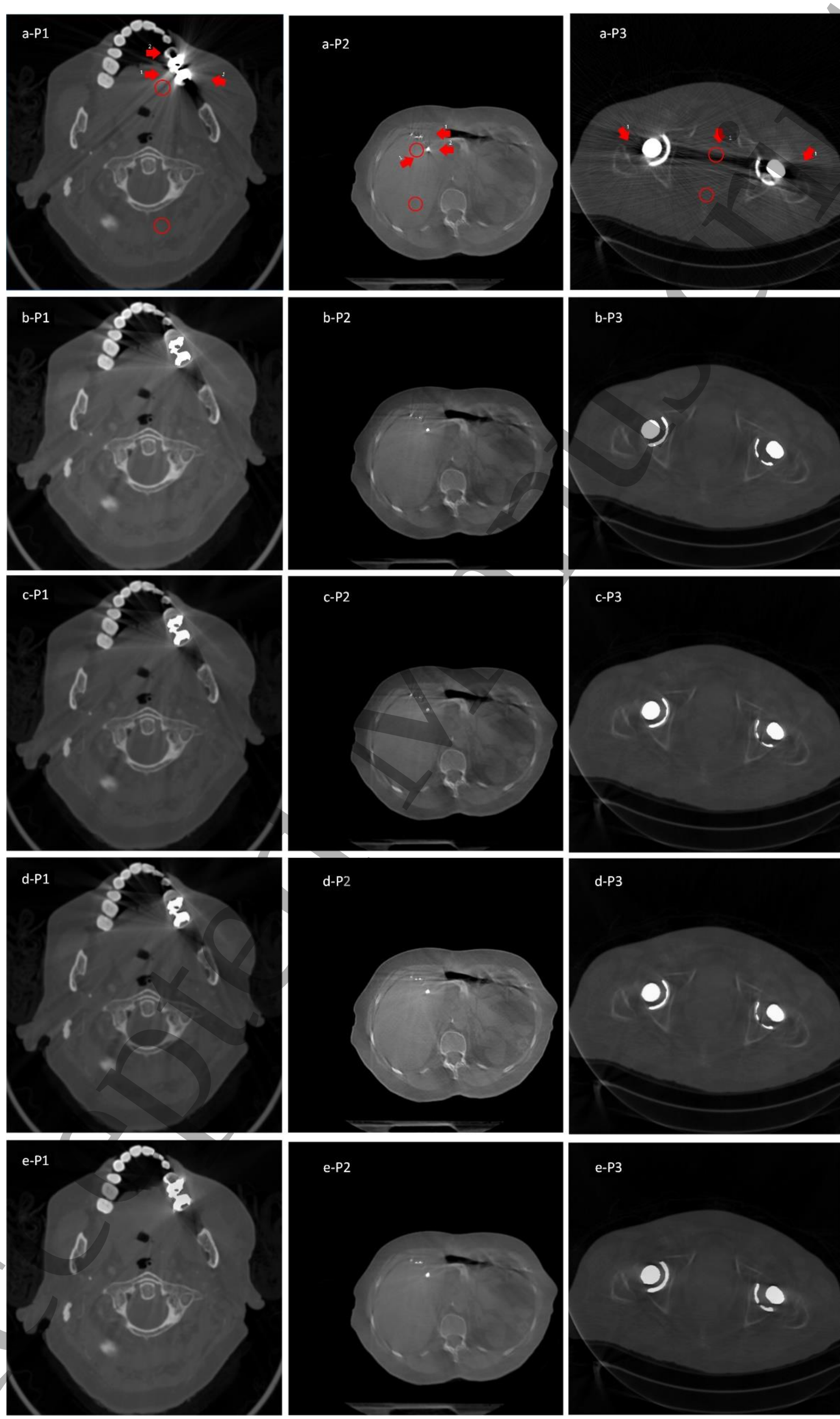

Accepted Manuscript

Fig. 2. Influence of the MAR algorithms on image quality. The ROI for assessment of the most severe artifact was placed at the location of the brightest streak artifact and in a segment weakly affected by artifacts. Left column: Patient I with dental filling, Middle column: Patient II with permanent seeds, Right column: Patient III with total hip implant. (a) The original artifact CT-slice (FBP) and the corrected images using the various MAR approaches: (b) LI, (c) NMAR, (d) FSNMAR and (e) GISMAR. Arrow 1 indicates the metal artifacts. Arrow 2 points at the recovery of edges and fine anatomical details. Window level: 300 HU; window width: 2,500 HU.

The diagnostic image quality was scored on CT-slices on a scale from 1 to 5 (1, severely reduced image quality, non-diagnostic; 2, markedly reduced image quality, with impaired diagnostic interpretability; 3, acceptable image quality and diagnostic interpretability; 4, good image quality, with high diagnostic confidence; 5, excellent image quality, with full diagnostic interpretability).

All numeric values were reported as the mean ± SD. For quantitative image quality assessment, paired and unpaired-t tests were used for comparison of ROI measurements between the algorithms, which were used because the Kolmogorov-Smirnov and Shapiro-Wilk tests revealed a distribution of data that was normal. In order to compare subjective image quality scores of the datasets, non-parametric Friedman-ANOVA was performed. P-values were adjusted for multiple comparisons using the Bonferroni-Holm method. With the purpose of assessing interobserver agreement, Cohen's kappa was used. The κ values of 0.01–0.20 were considered to indicate slight agreement, 0.21–0.40 for fair agreement, 0.41–0.60 for moderate agreement, 0.61–0.80 for substantial agreement and 0.81–1.00 for almost perfect agreement.

Statistical analyses were performed with statistical software (SPSS, version 22.0; IBM, Chicago, IL, USA). For all statistical analyses, p-values less than 0.05 were considered to represent statistically significant differences.

RESULTS

Quantitative image quality assessment

A comparison of HU values among the algorithms are shown in Table 1.

Table 1. Quantitative image quality analyses. Comparison between images reconstructed by FBP, LI, NMAR, FSNMAR and GISMAR algorithms.

	Total hips		**Permanent seeds**		**Dental Fillings**		**DBS**	
Algorithms	Segment with artifacts (HU)	Segment without artifacts (HU)	Segment with artifacts (HU)	Segment without artifacts (HU)	Segment with artifacts (HU)	Segment without artifacts (HU)	Segment with artifacts (HU)	Segment without artifacts (HU)

Accepted Manuscript

FBP	73.1 ± 12.5	51.9 ± 11.0	99.1 ± 12.5	70.1 ± 9.3	90.5 ± 9.8	62.1 ± 8.7	32.3± 11.3	32.3± 9.2
LI	68.7 ± 9.7	49.5 ± 12.1	83.8 ± 9.2	67.8 ± 10.1	71.3 ± 10.4	60.8± 8.9	22.8± 8.1	34.5± 7.2
NMAR	50.1 ± 9.3	49.2 ± 11.6	70.7 ± 9.4	67.2 ± 9.7	63.9 ± 10.5	61.3± 8.7	18.6± 6.2	32.6± 6.8
FSNMAR	50.2 ± 9.3	50.1 ± 9.9	70.5 ± 90.8	68.4 ± 8.2	62.4 ± 9.9	60.9± 8.2	18.4± 6.0	32.6± 6.9
GISMAR	49.8. ± 9.8	49.9 ± 9.5	69.5± 9.1	68.3 ± 7.8	61.6± 10.0	61.2 ± 8.3	19.0± 6.4	32.7± 6.6

For the ROI segments affected by metallic artifacts of any type, the mean HU values reconstructed by LI, NMAR, FSNMAR and GISMAR were better than those images reconstructed by FBP ($p < 0.001$ for all values). Specifically, for hip implants, there were significant differences among LI and all MAR algorithms ($p < 0.001$) due to the presence of some artifacts. The LI method does not reduce all artifacts and in some cases introduces new ones. Mean HU value showed a better performance of GISMAR method, but without significant differences with respect to the rest of MAR algorithms ($p> 0.05$).

For permanent seeds and total dental fillings, GISMAR presented good results, but there were not significant differences respect to FSNMAR ($p =0.120$ and $p=0.213$, respectively). For segments not affected by artifacts, mean HU values did not show significant differences ($0.105\leq p \leq 0.347$) among all reconstructed images.

In the case of patients with DBS implants, the worst algorithm was LI. There were no significant differences between NMAR, FSNMAR and GISMAR in areas not affected by artifacts. In areas close to the implant, FSNMAR was the best performing, although its differences were not significant regarding NMAR and GISMAR ($p =0.115$ and $p=0.354$, respectively).

Qualitative image quality assessment

Interobserver agreement for all assessments of image quality is shown in Table 2. The κ values for the three observers were from 0.638 to 0.8.24 for image quality in all the study. The worst agreement was between observer 1 and 2 with $\kappa = 0.655$ ($p < 0.001$) in presence of artifacts caused by permanent seeds.

Table 2. Comparison of interobserver agreement for all image quality assessment.

Total hip	**Observer 2**		**Observer 3**	
	κ	P	κ	P
Observer 1	0.801	<0.001	0.725	<0.001
Observer 2			0.705	<0.001

Permanent seed	**Observer 2**		**Observer 3**	
	κ	P	κ	P
Observer 1	0.655	<0.001	0.729	<0.001
Observer 2			0.678	<0.001

Accepted Manuscript

Dental Fillings	**Observer 2**		**Observer 3**	
	κ	P	κ	P
Observer 1	0.721	<0.001	0.730	<0.001
Observer 2			0.702	<0.001

DBS implants	**Observer 2**		**Observer 3**	
	κ	P	κ	P
Observer 1	0.824	<0.001	0.755	<0.001
Observer 2			0.762	<0.001

Table 3 shows the image quality among the algorithms. There were significant differences between all algorithms and BPF ($p < 0.001$). LI was the method with the worst result. The FSNMAR and NMAR methods had similar performances in all case studies. GISMAR had a similar performance to FSNMAR. Their main differences were in the regions close to the implant, where GISMAR had a better performance in patients with seed implants and FSNMAR in patients with DBS implants (Fig 6).

Table 3. Differences in image quality among the algorithms. P-values for pair-wise comparison of the different reconstruction techniques using Friedman-ANOVA and adjustment for multiple comparisons with the Bonferroni–Holms method.

Hip implants				
	LI	NMAR	FSNMAR	GISMAR
FBP	0.003	0.001	0.001	0.001
LI		0.002	0.018	0.001
NMAR			0.685	0.465
FSNMAR				0.505
Permanent seeds				
	LI	NMAR	FSNMAR	GISMAR
FBP	0.028	0.015	0.015	0.015
LI		0.020	0.020	0.020
NMAR			0.792	0.698
FSNMAR				0.505
Dental fillings				
	LI	NMAR	FSNMAR	GISMAR
FBP	0.004	0.001	0.001	0.001
LI		0.002	0.001	0.001
NMAR			0.652	0.425

Accepted Manuscript

FSNMAR				0.551
DBS implants				
	LI	NMAR	FSNMAR	GISMAR
FBP	0.046	0.001	0.001	0.001
LI		0.001	0.001	0.001
NMAR			0.701	0.695
FSNMAR				0.520

In patients with dental fillings, NMAR and FSNMAR algorithms reduced the streak artifacts, however the GISMAR algorithm tends to give a better suppression of the around teeth and restores more detail at a small distance from the artifacts. In Figure 3 is zoomed the tissues affected by artifacts and the results obtained by GISMAR.

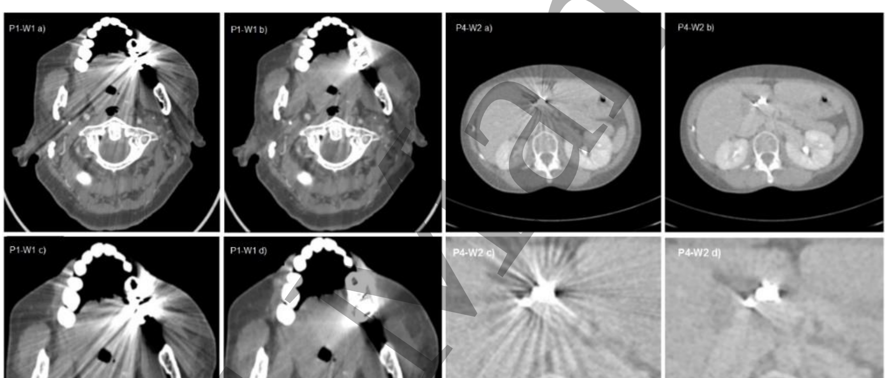

Fig. 3. Influence of the GISMAR algorithm on image quality. Reconstructions of a Patient 1 (P1) with several dental fillings and Patient 4 (P4) with seed implants. P1-W1 a) and P4-W2 a) were obtained from the FBP reconstructed DICOM CT-image; so as P1-W1 b) and P4-W2 b) were obtained from GISMAR. P1-W1 c) and P4-W2 c) were a zoom in the tissues affected by artifacts. Soft tissue was recovered and the method was able to recover edges and fine anatomical details, which are presented in P1-W1 d) and P4-W2 d). Images P1-W1 are displayed with window level 40 HU and window width 280 HU; and images P1-W2 with window level -100 HU and window width 400 HU.

On the other hand, a preliminary investigation was carried out on the advantages of using the final smoothing step in other MAR methods (Fig. 4). GISMAR method was able to reduce the artifacts efficiently, without its last step, keeping the details of the original image. This is due to the quality of the I^{Prior}, achieved with L0GM. However, the final quality was not good because the images were blurred, with noise, and the structures were not clearly visible. When the smoothing step was applied in LI, NMAR and FSNMAR methods, with the same parameters used in GISMAR, there was a reduction in the blurring of

Accepted Manuscript

the images and some structures were observed better, which was more evident in FSNMAR method. However, some streaks are reintroduced by LI, NMAR and FSNMAR.

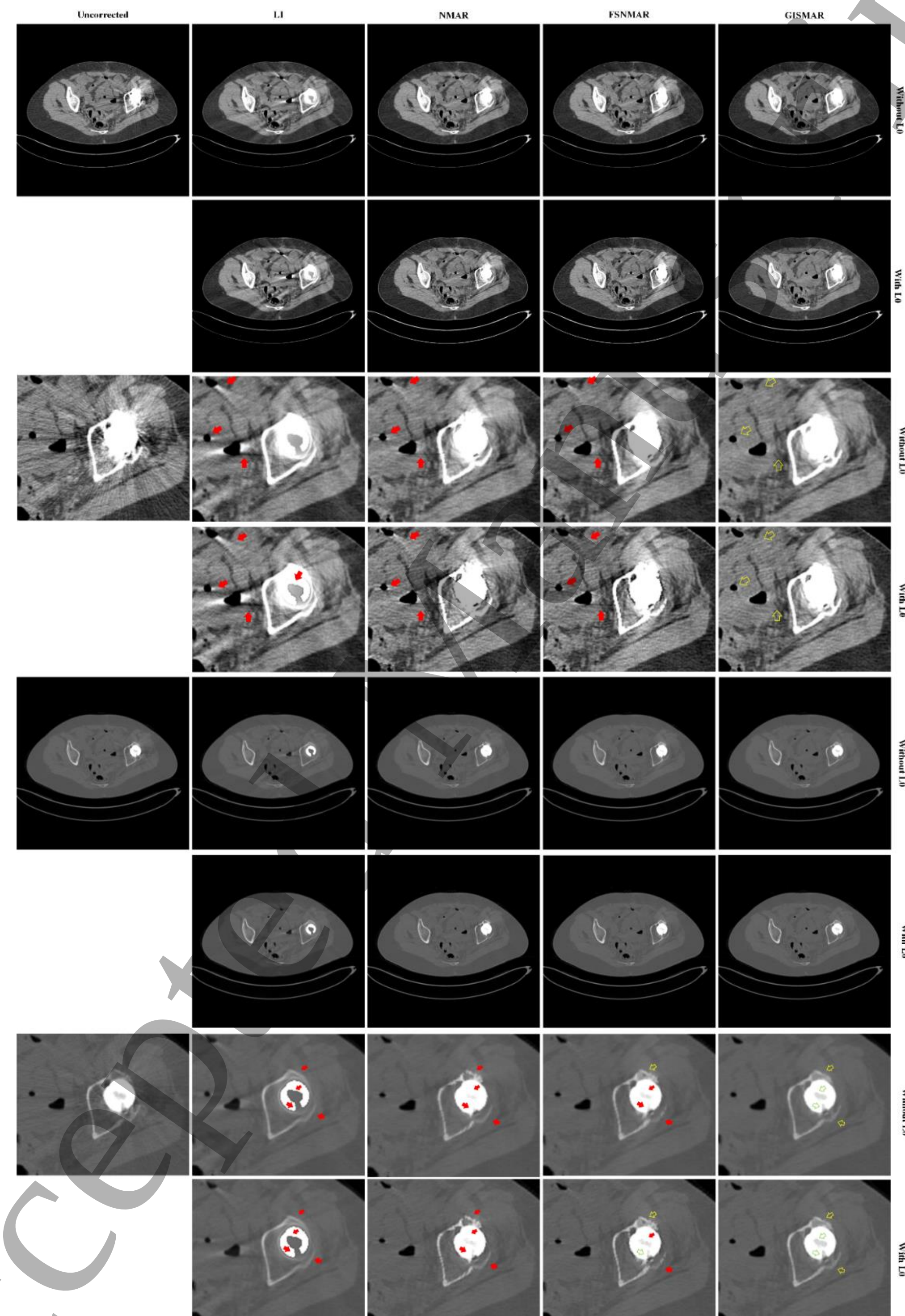

Fig. 4. Patient with unilateral total hip replacement. Red arrows are used in the magnified images to mark the position where the anatomical details are lost or exist artifacts. White arrows are used to highlight the

Accepted Manuscript

position where corresponding details are restored or the artifacts are reduced. Using the final smoothing step of GISMAR, some slight streaks are reintroduced by LI, NMAR and FSNMAR, but the blurring is removed; and bone structures were restored by FSNMAR. GISMAR yields the best correction. Top four rows: window level 10 HU and window width 450 HU, bottom four rows: window level 300 HU and window width 2500 HU.

From the expert observer's point of view, if small metal objects such as permanent seeds were within the field of measurement, GISMAR were more susceptible to artifacts reduction than LI, NMAR, FSNMAR and FBP. In addition, GISMAR was able to improve image quality in pelvis; and recover the delineation of the tissues neighboring the metal hardware (Fig. 4).

The GISMAR method was developed to work on reconstructed images on axial slice. However, when the artifacts have been reduced in all the slices, it is possible to build a 3D volume. Figure 5 shows axial, sagittal and coronal slices obtained after the application of GISMAR method in a patient with unilateral total hip replacement.

Fig. 5. Example of patient with unilateral total hip replacement. Axial, coronal and sagittal images before correction with FBP and GISMAR algorithm are displayed at window level 10 HU, window width 450 HU; and window level 300 HU, window width 2500 HU.

Additionally, experiments with GISMAR method were conducted with CT-slices that were severely deteriorated to know its performance. This is the case of the patient with DBS implant presented in Fig. 6. This dataset was affected by noise, metal artifacts and beam hardening. The experiments showed that GISMAR was able to reduce noise and metal artifacts. However, it was not able to recover the structures in the vicinity of the implant. LI was the worst performing method. The performance of FSNMAR and NMAR algorithms was poor, because new artifacts were introduced.

Accepted Manuscript

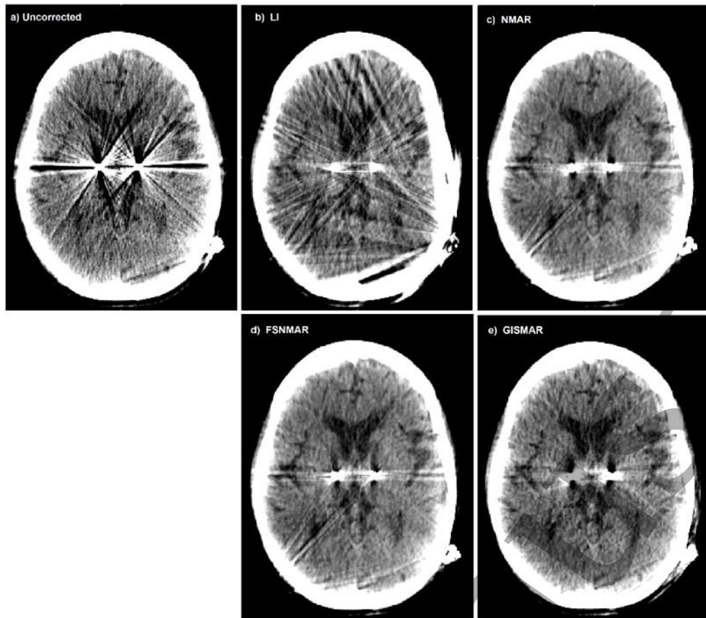

Fig. 6. Patient with DBS implant. Window level: 0 HU; window width: 1000 HU.

An evaluation on the spatial resolution among MAR methods was carried out. Figure 7 shows the analysis performed for the patient dataset with unilateral total hip replacement presented in Fig. 4. The Modulation Transfer Function (MTF) [32] was estimated for two different ROI. For ROI a), close to the artifact, the area under the MTF curves decreases more than for ROI b), distant from artifact, as consequence of the MAR method used. In both cases, the method that had the MTF closest to the uncorrected image was GISMAR, and the method that had the worst MTF was LI.

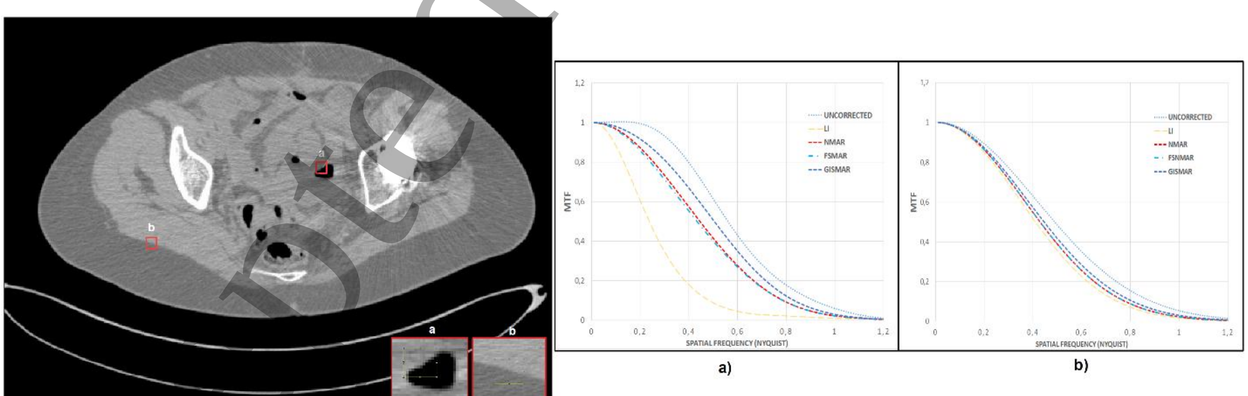

Fig. 7. MTF versus spatial frequency for MAR methods in a patient with unilateral total hip replacement. ROI a) close to the artifact. ROI b) distant from artifact. Window level 0 HU, window width 1000 HU.

Accepted Manuscript

DISCUSSION

In this paper, a new procedure to reduce metal artifacts was proposed. The core of the GISMAR algorithm revolves around the combination of prior image creation and Gaussian smoothing filter application, the result of which is then interpolated obtaining the reconstructed image. Finally, this image is smoothed using L0GM to improve its quality.

In presence of high-density objects, such as metals, the effects of beam hardening, scattered radiation, photon starvation and noise cause the FBP algorithm to produce reconstructions characterized by artifacts. LI was able to improve the overall image quality, but this algorithm still induced artifacts which negatively influenced the diagnostic confidence in the assessment. NMAR was able to improve image quality and proved to be superior to both FBP and LI. However, it still suffers from loss of details close to metal implants and it is dependent on a good prior image with accurate segmentation [12]. On the other hand, GISMAR can restore structures between or in the neighborhood metal implants better than or similar to FSNMAR. This algorithm is able to recover clear edges and fine anatomical details.

The addition of the final smoothing step (L0GM method) in all MAR methods improved the delineation of the tissues neighboring in the metal hardware (muscles, tendons and joint) and the implant itself. Both FSNMAR and GISMAR improved the image quality. More investigations about the application of L0GM in MAR methods should be carry out in the future.

A good prior image is important to perform the normalization process. Parameters selection for obtaining a prior image and metal image are usually chosen empirically in some methods [12, 13, 24]. The κ values should be close to 2 according to the authors of L0GM, to achieve the best results [21]. GISMAR uses κ = 1.8. This parameter was varied up to 2%, observing that the differences were not visually perceptible. However, in dependence on the body region, the energy spectrum used for the CT acquisition changes. Higher values of kVp increases the X-ray penetration and the variation of the whole image contrast. In the present study, only three values of kVp were tested. The factors *ThF1* and *ThF2* were determined with the purpose of GISMAR method was scalable and depend on few parameters for its future implementation, but they should be experimentally fitted. New studies on the tuning of *ThF1* and *ThF2* factors with other datasets, and from different CT scanners will be carried out in the future.

The value of λ is also conditioned by the acquisition parameters, mainly the mAs, which essentially determine the noise. More iterations could yield an over-smoothing, losing image information. In general terms, lower values of mAs imply higher values of λ. This parameter also should be experimentally fitted, according to the acquisition protocol used.

Accepted Manuscript

The GISMAR algorithm makes use of L0GM. This method enhances edges and preserves the tissue characteristics, reducing the noise. GISMAR does not perform iterative reconstruction, as these are time consuming. The average time needed to obtain the final image was approximately of 50 seconds on an Intel Core i5, CPU 1.8-GHz PC.

The GISMAR algorithm also has advantages for clinical work flow. It has the ability to operate directly on DICOM CT-slices, reducing the artifacts and improving image quality. Many MAR algorithms require access to raw projection data, but these often cannot be implemented on commercial CT scanners due to restrictions. From this algorithm, a dedicated software for using in workstations by radiologists could be developed, even for personal laptops.

Despite the large number of iterative reconstruction algorithms developed in recent years, and the increase in computational power of the equipment, even these are not able to significantly reduce metal artifacts. Geyer *et al* [33] describe the currently available algorithms published by some CT manufacturers, observing that the results obtained are not yet satisfactory. On the other hand, Sunwoo *et al* [34] evaluated the performance of the metal artifact reduction for orthopedic implants (O-MAR) in patients with intracranial metallic implants, concluding that in many cases the reduction of the streak artifacts was not significant. The application of hybrid techniques, a combination of iterative reconstruction algorithms and algorithms that works in image domain, could be a solution for the reduction of metal artifacts.

The main limitation of the present contribution is the number of images studied. It would be important to increase the sample for a more elaborate evaluation of the algorithm performance, as well as to investigate other common sources of streaking artifacts, such as spinal screws.

In conclusion, the results in this paper show that GISMAR algorithm reduces streak artifacts and restores the CT numbers of the tissues surrounding the metal. In the comparison, it was observed that GISMAR had a similar performance to FSNMAR algorithm, although in some cases, it was able to recover with more precision the details surrounding the implants. In addition, it was found that GISMAR tends to avoid the introduction of new artifacts in CT-slices. A clinical study involving more cases is preparing to prove the effectiveness of GISMAR.

Acknowledgements

The authors would like to thank Professor Dr. Norbert Pelc from Stanford University and Dr. Samuel Mazin from RefleXion Medical for provide clinical data. We sincerely thank Armando Alaminos for his collaboration.

Compliance with ethical standards

Accepted Manuscript

Yakdiel Rodríguez-Gallo, Rubén Orozco-Morales and Marlen Pérez-Díaz declare that they have no conflict of interest.

The authors state that this work has not received any funding. All procedures performed in studies involving human participants were in accordance with the ethical standards of the institutional and/or national research committee and with the 1964 Helsinki declaration and its later amendments or comparable ethical standards. Informed consent was obtained from all individual participants included in the study.

References

1. Hamie QM, Kobe AR, Mietzsch L, et al (2018) Prototype metal artefact reduction algorithm in flat panel computed tomography - evaluation in patients undergoing transarterial hepatic radioembolisation. Eur Radiol 28:265–273. https://doi.org/10.1007/s00330-017-4946-1

2. Giantsoudi D, De Man B, Verburg J, et al (2017) Metal artifacts in computed tomography for radiation therapy planning: dosimetric effects and impact of metal artifact reduction. Phys Med Biol 62:R49–R80. https://doi.org/10.1088/1361-6560/aa5293

3. Kennedy JA, Israel O, Frenkel A, et al (2007) The reduction of artifacts due to metal hip implants in CT-attenuation corrected PET images from hybrid PET/CT scanners. Med Bio Eng Comput 45:553–562. https://doi.org/10.1007/s11517-007-0188-8

4. Gjesteby L, Man BD, Jin Y, et al (2016) Metal Artifact Reduction in CT: Where Are We After Four Decades? IEEE Access 4:5826–5849. https://doi.org/10.1109/ACCESS.2016.2608621

5. Kuchenbecker S, Faby S, Sawall S, et al (2015) Dual energy CT: how well can pseudo-monochromatic imaging reduce metal artifacts? Med Phys 42:1023–1036. https://doi.org/10.1118/1.4905106

6. Bamberg F, Dierks A, Nikolaou K, et al (2011) Metal artifact reduction by dual energy computed tomography using monoenergetic extrapolation. Eur Radiol 21:1424–1429. https://doi.org/10.1007/s00330-011-2062-1

7. Hahn K, Schöndube H, Stierstorfer K, et al (2016) A comparison of linear interpolation models for iterative CT reconstruction. Med Phys 43:6455–6473. https://doi.org/10.1118/1.4966134

8. Rajwade J, Miller L, Simon D (2012) Partial-data interpolation method for arc handling in a computed tomography scanner. Comput Med Imag Grap 36:387–395. https://doi.org/10.1016/j.compmedimag.2012.04.004

9. Yu H, Zeng K, Bharkhada DK, et al (2007) A Segmentation-Based Method for Metal Artifact Reduction. Acad Radiol 14:495–504. https://doi.org/10.1016/j.acra.2006.12.015

10. Glover GH, Pelc NJ (1981) An algorithm for the reduction of metal clip artifacts in CT reconstructions. Med Phys 8:799–807. https://doi.org/10.1118/1.595032

11. Mahnken AH, Raupach R, Wildberger JE, et al (2003) A new algorithm for metal artifact reduction in computed tomography: in vitro and in vivo evaluation after total hip replacement. Invest Radiol 38:769–775. https://doi.org/10.1097/01.rli.0000086495.96457.54

Accepted Manuscript

12. Meyer E, Raupach R, Lell M, et al (2010) Normalized metal artifact reduction (NMAR) in computed tomography. Med Phys 37:5482–5493. https://doi.org/10.1118/1.3484090

13. Meyer E, Raupach R, Lell M, et al (2012) Frequency split metal artifact reduction (FSMAR) in computed tomography. Med Phys 39:1904–1916. https://doi.org/10.1118/1.3691902

14. Lell MM, Meyer E, Schmid M, et al (2013) Frequency split metal artefact reduction in pelvic computed tomography. Eur Radiol 23:2137–2145. https://doi.org/10.1007/s00330-013-2809-y

15. Wang G, Frei T, Vannier MW (2000) Fast iterative algorithm for metal artifact reduction in X-ray CT. Acad Radiol 7:607–614. https://doi.org/10.1016/S1076-6332(00)80576-0

16. Zhang H, Wang L, Li L, et al (2016) Iterative metal artifact reduction for x-ray computed tomography using unmatched projector/backprojector pairs. Med Phys 43:3019–3033. https://doi.org/10.1118/1.4950722

17. Brabant L, Pauwels E, Dierick M, et al (2012) A novel beam hardening correction method requiring no prior knowledge, incorporated in an iterative reconstruction algorithm. NDT & E Int 51:68–73. https://doi.org/10.1016/j.ndteint.2012.07.002

18. Dong J, Kondo A, Abe K, Hayakawa Y (2011) Successive iterative restoration applied to streak artifact reduction in X-ray CT image of dento-alveolar region. Int J CARS 6:635–640. https://doi.org/10.1007/s11548-010-0544-2

19. Fang J, Zhang D, Wilcox C, et al (2017) Metal implants on CT: comparison of iterative reconstruction algorithms for reduction of metal artifacts with single energy and spectral CT scanning in a phantom model. Abdom Radiol 42:742–748. https://doi.org/10.1007/s00261-016-1023-1

20. Naranjo V, Lloréns R, Alcañiz M, López-Mir F (2011) Metal artifact reduction in dental CT images using polar mathematical morphology. Comput Methods Programs Biomed 102:64–74. https://doi.org/10.1016/j.cmpb.2010.11.009

21. Xu L, Lu C, Xu Y, Jia J (2011) Image Smoothing via L0 Gradient Minimization. ACM Trans Graph 30:174:1–174:12. https://doi.org/10.1145/2070781.2024208

22. Bianconi F, Fernández A, González E, Ribas F (2007) Texture Classification Through Combination of Sequential Colour Texture Classifiers. In: Progress in Pattern Recognition, Image Analysis and Applications. pp 231–240

23. Bianconi F, Ceccarelli L, Fernández A, Saetta SA (2014) A sequential machine vision procedure for assessing paper impurities. Comput Ind 65:325–332. https://doi.org/10.1016/j.compind.2013.12.001

24. Kalender WA, Hebel R, Ebersberger J (1987) Reduction of CT artifacts caused by metallic implants. Radiol 164:576–577. https://doi.org/10.1148/radiology.164.2.3602406

25. Fernández A, Ghita O, González E, et al (2017) Evaluation of robustness against rotation of LBP, CCR and ILBP features in granite texture classification. Mach Vis Appl 22:913–926. https://doi.org/10.1007/s00138-010-0253-4

Accepted Manuscript

26. Li Y, Bao X, Yin X, et al (2010) Metal artifact reduction in CT based on adaptive steering filter and nonlocal sinogram inpainting. In: Biomedical Engineering and Informatics (BMEI), 2010 3rd International Conference on. IEEE, pp 380–383

27. Liu X, Mei W, Du H (2016) Multimodality medical image fusion algorithm based on gradient minimization smoothing filter and pulse coupled neural network. Biom Sig Proces 30:140–148. https://doi.org/10.1016/j.bspc.2016.06.013

28. Duan Y, Chang H, Huang W, et al (2015) The L0 Regularized Mumford-Shah Model for Bias Correction and Segmentation of Medical Images. IEEE Trans Image Process 24:3927–3938. https://doi.org/10.1109/TIP.2015.2451957

29. Karimi S, Cosman P, Wald C, Martz H (2012) Segmentation of artifacts and anatomy in CT metal artifact reduction. Med Phys 39:5857–5868. https://doi.org/10.1118/1.4749931

30. Zhang Y, Yan H, Jia X, et al (2013) A hybrid metal artifact reduction algorithm for x-ray CT. Med Phys 40:4. https://doi.org/10.1118/1.4794474

31. Golden C, Mazin SR, Boas FE, et al (2011) A comparison of four algorithms for metal artifact reduction in CT imaging. In: Proc. SPIE. p 79612Y

32. Park SK, Schowengerdt, R, Kaczynski M-A (1984) Modulation-transfer-function analysis for sampled image systems. Applied optics 23:2572–2582. https://doi.org/10.1364/AO.23.002572

33. Geyer LL, Schoepf UJ, Meinel FG, et al (2015) State of the Art: Iterative CT Reconstruction Techniques. Radiology 276:339–357. https://doi.org/10.1148/radiol.2015132766

34. Sunwoo L, Park S-W, Rhim JH, et al (2018) Metal Artifact Reduction for Orthopedic Implants: Brain CT Angiography in Patients with Intracranial Metallic Implants. Journal of Korean Medical Science 33:. https://doi.org/10.3346/jkms.2018.33.e158

Accepted Manuscript